

Enhanced coercivity and emergent spin-cluster-glass state in 2D ferromagnetic material, Fe_3GeTe_2

Satyabrata Bera,¹ Suman Kalyan Pradhan,¹ Riju Pal,² Buddhadeb Pal,² Arnab Bera,¹ Sk Kalimuddin,¹ Manjil Das,¹ Deep Singha Roy,¹ Hasan Afzal,¹ Atindra Nath Pal,² and Mintu Mondal^{1,*}

¹*School of Physical Sciences, Indian Association for the Cultivation of Science, Jadavpur, Kolkata 700032, India*

²*SN Bose National Centre for Basic sciences, Sector III, Block JD, Salt Lake, Kolkata 700106, India.*

(Dated: January 2, 2023)

Two-dimensional (2D) van der Waals (vdW) magnetic materials with high coercivity and high T_C are desired for spintronics and memory storage applications. Fe_3GeTe_2 (F3GT) is one such 2D vdW ferromagnet with a reasonably high T_C , but with a very low coercive field, H_c ($\lesssim 100$ Oe). Some of the common techniques of enhancing H_c are by introducing pinning centers, defects, stress, doping, etc. They involve the risk of undesirable alteration of other important magnetic properties. Here we propose a very easy, robust, and highly effective method of phase engineering by altering the sample growth conditions to greatly enhance the intrinsic coercivity (7-10 times) of the sample, without compromising its fundamental magnetic properties ($T_C \simeq 210\text{K}$). The phase-engineered sample (F3GT-2) comprises of parent F3GT phase with a small percentage of randomly embedded clusters of a coplanar FeTe (FT) phase. The FT phase serves as both mosaic pinning centers between grains of F3GT above its antiferromagnetic transition temperature ($T_{C1} \sim 70$ K) and also as anti-phase domains below T_{C1} . As a result, the grain boundary disorder and metastable nature are greatly augmented, leading to highly enhanced coercivity, cluster spin glass, and meta-magnetic behavior. The enhanced coercivity ($\simeq 1$ kOe) makes F3GT-2 much more useful for memory storage applications and is likely to elucidate a new route to tune useful magnetic properties. Moreover, this method is much more convenient than hetero-structure and other cumbersome techniques.

I. INTRODUCTION

The magnetic materials are an integral part of modern-day technologies, based on desired application-oriented magnetic properties such as saturation magnetization (M_s), remanent magnetization, and coercivity (H_c)[1, 2]. The two-dimensional (2D) van der Waals (vdW) materials have recently emerged as potential candidates for technological applications [3–6]. However, the typical Curie temperatures and coercivity of these vdW magnetic materials are low compared to their three-dimensional (3D) counterparts [7].

Recently, the family of Fe_nGeTe_2 ($n = 3, 4, 5$) (FnGT) vdW compounds [8–11] are found to be both metallic [12] and ferromagnetic (FM) with reasonably, higher T_C ($\gtrsim 200$ K) compared to other reported families of FM vdW materials [13–16]. Moreover, this family of vdW FM materials hosts complex magnetic phases with complex spin textures [10] and emerged as versatile scientific platforms for studying various novel quantum phenomena[17–19]. The Fe_3GeTe_2 (F3GT) is a well-studied compound of this family, because of the following features - (i) Easy to grow a few millimeter-sized crystals, (ii) Transition temperature, T_C can easily be tuned in the range, 150-230 K by varying Fe concentration (i.e. x in $\text{Fe}_{3-x}\text{GeTe}_2$) [20], (iii) Observation of novel phenomena, like heavy-fermion state[21], strong electron correlation effect[20] and (iv) manipulable magnetic domain[22]. These properties make F3GT an important scientific platform for further research to enhance

T_C and coercivity (H_c) for potential applications. A recent study revealed that intercalation of F3GT with sodium and TBA+ molecules leads to a ferromagnetic ordering above room temperature ($T > 300$ K) [23, 24]. Very recently L. Zhang *et.al.*, have reported an improvement of ferromagnetic transitions temperature, T_C in the heterostructure of Fe_3GeTe_2 and FePS_3 [25] due to the proximity coupling effect, which modifies the spin textures of F3GT at the interface.

However, the low H_c value of F3GT is a significant hindrance to the realization of prospective technological applications[26]. The coercivity (H_c) is the measure of the ability of a ferromagnetic material to withstand an external perturbation without becoming demagnetized. Based on the value of coercivity (H_c), magnetic materials are classified into two segments, soft and hard ferromagnets. Soft magnets generally show coercivity (H_c) in the Oe range, whereas later is in the order of kOe range. Soft magnets are required in applications such as switching, sensing, and microwave absorbing medium [27, 28], whereas, hard magnets are useful in motors, generators, and data storage devices[29]. Therefore, the search for new high-performance magnetic materials based on transition metals (free from costly rare earth elements), in particular, 2D vdW magnetic materials with high H_c has been the research focus for the past decade [30]. The high H_c can be tuned or obtained from the combination of several factors, such as intrinsic magnetic interaction [31, 32], high pressure[33], doping[34–37], pinning effect by defects or stress[38–40], and shape anisotropy[41, 42] of nanosheets due to their 2D nature. However, all these methods involve cumbersome synthesis and application procedures and also may alter other important magnetic

* sspmm4@iacs.res.in

properties of the sample including T_C , saturation magnetization values, etc., all of which are undesirable from the application point of view. To our knowledge, there are no reports regarding the enhancement of H_c value in the parent F3GT compound subject to different growth techniques. Tuning growth techniques to synthesize F3GT and subordinate compounds to enhance the required critical coercive field (H_c) can be a promising way for the development of 2D vdW magnetic materials with a high coercive field. Additionally, by tuning of synthesis condition, one can introduce controlled defects, impose disorder, and change the particle size in the compound, leading to the emergence of many novel magnetic phenomena such as exchange bias effect[43], glassy, and superparamagnetic state[44] which are not only important for fundamental understanding but also bear technological relevance.[45–49]

Here, we demonstrate a very easy, robust, and highly effective method of phase engineering by altering the sample growth conditions to greatly enhance the intrinsic coercivity (7-10 times) of the sample, without compromising its fundamental magnetic properties ($T_C \sim 210$ K). Using the method of phase engineering, by altering the sample growth conditions and initial reactant stoichiometry (mentioned in detail in the manuscript), we have successfully been able to enhance the intrinsic coercivity of the sample by an order of magnitude, up to temperatures close to T_C , without any reduction in T_C and other parameters. The phase-engineered version (F3GT-2) comprises of parent F3GT phase with a small percentage of randomly embedded clusters of a co-planar FeTe (FT) phase, which serve as both mosaic pinning centers between grains of F3GT above the antiferromagnetic transition of FT ($T_{C1} \sim 70$ K) and also as anti-phase domains below T_{C1} .

A comparative magnetic and magnetotransport study of parent F3GT (F3GT-1) along with the phase-engineered version (F3GT-2) has been performed. The samples were grown using the chemical vapor transport (CVT) method. Single-crystal x-ray diffraction results confirm F3GT-1 as single-phased, whereas F3GT-2 shows a 1.2% FeTe (FT) phase, which has been deliberately added by altering the growth conditions. The 2-phase structure in F3GT-2 is further verified by electrical transport measurements B. In addition to increased coercivity, other new interesting phenomena, such as cluster glass (CG) and meta-magnetic behavior have also been observed in F3GT-2. The coercive field of F3GT-2 has been successfully enhanced to 7-10 times the value of H_c of F3GT-1. This study demonstrates an effective way to significantly enhance the coercivity of 2D VdW ferromagnetic materials in general, for prospective potential applications.

II. EXPERIMENTAL DETAILS

Two batches of F3GT samples (labeled as F3GT-1 and F3GT-2) were grown in single crystal form by chemical vapor transport (CVT) method with I_2 as trans-

port agent in both cases. The high-purity elements: Fe (99.99% pure), Ge (99.99% pure) and Te (99.99% pure) powder were used as starting materials. To grow good quality F3GT crystals (i.e. F3GT-1), the powders were mixed stoichiometrically (molar ratio, Fe : Ge : Te = 3 : 1 : 2) and grind thoroughly in an agate motor. Then 5 mg-cm⁻³ I_2 powder was added to the mixture and placed in a quartz tube. The tube was sealed under a vacuum of 2×10^{-4} mb, thereafter the sealed quartz tube was placed horizontally in a two-zone horizontal tube furnace for seven days, keeping the hot-end at 750°C and cold-end at 700°C, respectively. F3GT-2 crystals were also prepared by the same method with different temperature gradients (cold zone at 700°C and hot zone at 800°C). Shining single crystals with dimensions $2 \times 1.5 \times 0.1$ mm³ and $2.5 \times 2.5 \times 0.5$ mm³ were obtained at the cold-end for both the cases respectively[13, 50]. The phase composition and crystal structure were investigated by the standard X-ray diffraction (XRD) technique using Rigaku diffractometer equipped with Cu- K_α radiation ($\lambda = 1.54056$ Å). The micro-morphology was characterized with a field emission scanning electron microscope (FE SEM, JEOL LSM-6500). The elemental composition analysis of both samples was done by taking x-ray energy-dispersive spectroscopy (EDS). Electrical transport measurements were carried out by an Oxford Instrument cryogenic system with a conventional dc measurement method, from 5 K - 300 K. Magnetic studies ($M-T$, $M(H)$, and $M-t$) were done using Magnetic Properties Measurement System (MPMS-SQUID) in the temperature interval of 2 K-300 K, up to 50 kOe magnetic field H . The plate-like single crystals were used to minimize the misalignment of samples during these measurements.

III. RESULTS

A. XRD analysis and crystal structure

The room temperature single-crystal XRD patterns of F3GT-1 and F3GT-2 are shown in Figure 1(a). Powder XRD data of the F3GT-1 sample are well fitted the P63/mmc space group and lattice parameters are $a = 3.96$ Å and $c = 16.36$ Å (detail analysis are presented in Figure 1(b)). In the single-crystal XRD pattern, all peaks come from (00 l), which indicates that the crystal surface is normal to the c axis with the plate-shaped surface parallel to the ab plane. Besides, the most important point is that two small peaks are observed for F3GT-2 (see Figure 1(a)) around $2\theta = 60^\circ$. These secondary peaks indicate the existence of the FeTe phase[51]. By comparing with the profile peak the obtained percentage of the secondary phase is 1.22%. The crystal structure of F3GT-1 is shown inset of the Figure 1(b), which contains Fe₃Ge slabs isolated by van der Waals bonded Te double layers. The Fe atoms in the unit cell contain two non-identical Wyckoff sites Fe1 and Fe2, as shown in the inset of the Figure 1(b). The Fe1 atoms are situated in a hexagonal net in a layer with only Fe atoms. The Fe2 and Ge atoms are covalently bonded in an adjacent layer[8, 52].

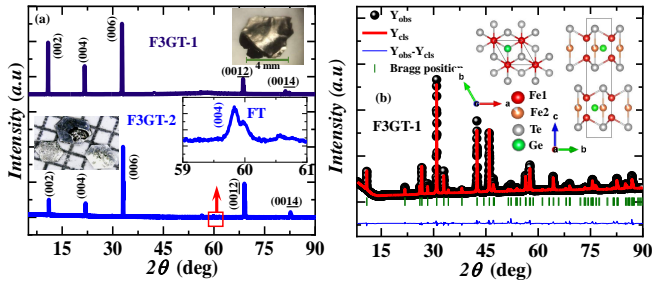


FIG. 1 Structural analysis of F3GT crystal.

(a) The X-ray diffraction pattern obtained from the cleaved plane of F3GT (F3GT-1 & F3GT-2) single crystals at room temperature. The picture of the single crystal is shown in the inset. (b) Observed (solid black sphere) and calculated (solid red line) powder X-ray-diffraction patterns for the powder F3GT-1 crystals. The green short lines denote the Bragg positions, and the blue curve indicates the difference between the observed and calculated patterns. View of the crystallographic structure of F3GT-1 from the a axis and c axis. The ash, red, and green spheres represent the Te, Fe and Ge respectively. The black box with the cross-section rectangles depicts a crystallographic unit cell.

TABLE I Crystallographic parameters obtained from a Rietveld refinement of the powder x-ray diffraction pattern collected at room temperature for a polycrystalline sample with a nominal composition Fe_3GeTe_2 (F3GT-1)

Nominal composition	Fe_3GeTe_2				
Refined composition	$\text{Fe}_{2.88}\text{GeTe}_2$				
Structure	Hexagonal				
Space group	$P6_3/mmc$ (No. 194)				
Formula units/unit cell (Z)	2				
Lattice parameters					
a (\AA)	3.96148				
b (\AA)	3.96148				
c (\AA)	16.3812				
V_{cell} (\AA^3)	222.6339				
Atom	Wyckoff position	x	y	z	Occupancy
Fe1	4e	0	0	2/3	1
Fe2	2c	2/3	1/3	3/4	0.882
Ge1	2d	1/3	2/3	3/4	1
Te1	4f	2/3	1/3	0.58709	1

By contrast, our EDX result gives Fe deficiencies and Te excess for F3GT-1 with a composition of $\text{Fe}_{2.84}\text{GeTe}_{2.1}$ and for F3GT-2 with a composition of $\text{Fe}_{2.94}\text{GeTe}_{2.12}$.

B. Magnetic properties of F3GT:

1. Magnetization vs temperature measurements

The dc magnetic susceptibility ($\chi_{dc} = M/H$) of both samples have been measured in the zero-field-cooled (ZFC), field cool cooling (FCC), and field-cool-heating (FCH) protocols under applied magnetic fields (H) in the temperature range 2 to 300 K. Figure 2(a-b) shows the M - T data of F3GT-1 at applied magnetic field, $H = 100$ Oe in ab plane and parallel to the c axis, respectively. Initially, the susceptibility increases slowly with decreasing temperature demonstrating a typical paramagnetic (PM) nature. With a further decrease in temperature, the susceptibility rapidly increases at around T_C , revealing the onset of a ferromagnetic (FM) ordering[8, 13, 52]. The effective magnetic moment of F3GT-1 is calculated from by fitting the $M/H(T)$ data (using $H = 0.1$ kOe FCC data) using following modified *Curie-Weiss* (C-W) law,

$$\frac{M}{H} = \chi_0 + \frac{C}{(T - \Theta_p)} \quad (1)$$

in the temperature range 240-300 K, where C is the Curie constant and Θ_p is the C-W temperature (see inset of Figure 2(a)). The obtained effective magnetic moment (μ_{eff}) and C-W temperature (Θ_p) from the fit are $4.54 \mu_B/\text{f.u.}$ and 162 K for $H \parallel ab$, respectively. Similarly, we have obtained (μ_{eff}) = $4.61 \mu_B/\text{f.u.}$ and $\Theta_p = 178$ K for $H \parallel c$ direction(see inset of Figure 2(b)). The positive value of Θ_p indicates the prominent FM interaction of the compound. These effective moment values are in good agreement with earlier reports[8, 53].

The first derivative of χ_{dc} w.r.t T ($d\chi_{dc}/dT$) data of F3GT-1 along the ab plan (see the Figure C (a-b) in appendix) reveals another two magnetic ordering at around $T_{C1} = 142$ K and $T_{C2} = 6$ K. The above signatures in susceptibility data strongly suggest complex nature of the magnetic ground state in F3GT with novel magnetic properties [10].

Figure 2(c-d) presents the $\chi_{dc}(M/H)$ - T nature of F3GT-2 at $H = 0.1$ kOe, in ab plane and parallel to the c axis, respectively and shows a ferromagnetic ordering at T_C . The $d\chi_{dc}/dT$ vs T for F3GT-2 suggests that besides FM transition, there exists another magnetic ordering at around 70 K (see appendix C) confirming the presence of FT phase as observed in XRD study [51, 54]. The ZFC and FCC plots show significant splitting below 210 K for $H \parallel ab$ and $H \parallel c$ directions. The extent of bifurcation between FCC and ZFC data also increases with decreasing values of H (for details see appendix C). Such behavior is often observed in disordered or glassy magnetic systems. Below $T_C = 210$ K, the value of χ_{dc} for $H \parallel c$ axis is about eleven times larger than it for $H \parallel ab$ plane, which indicates the anisotropic behavior in the ordered state [52, 55]. The high-temperature (240-300

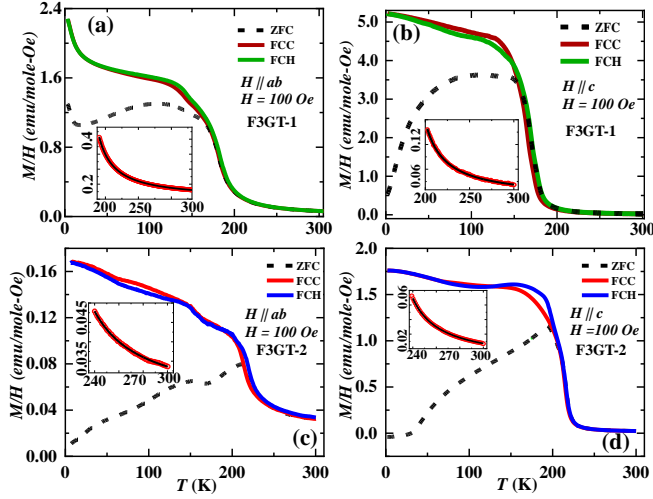


FIG. 2 Temperature dependent magnetization measurements. Magnetization measured at external magnetic field $H = 0.1$ kOe applied in the ab plane and along the c axis under zero-field-cooling (ZFC), field-cooling (FC) and field-cool-heating (FCH) protocols for (a-b) F3GT-1 and (c-d) F3GT-2. The inset shows modified Curie-Weiss fits to the magnetic susceptibility data.

K) M/H data is fitted (see the inset of Figure 2(c-d)) using modified Curie-Weiss law (equation 1). The obtained paramagnetic moment is μ_{eff} to be $2.94\mu_B$ /(f.u. of $\text{Fe}_{2.94}\text{GeTe}_{2.1}$), and $\Theta_p = 208\text{K}$ for $H \parallel c$ and 198K for $H \parallel ab$. The value of χ_0 is found to be small but positive [8, 55].

2. Magnetization vs applied magnetic field measurements: M - H loops

To shed light on the nature of the magnetic phase, measurement of magnetization as a function applied magnetic field was carried out at various temperatures, as shown in Figure 3. The isothermal M vs H curves of F3GT-1 sample at a few selected temperatures ($T=2, 180$ and 300 K) in ab plane and along c -axis are presented in Figure 3(a and b) respectively. The saturation behavior is observed in both directions. The saturation fields at 2 K are $H_c^s \approx 3.34$ kOe for $H \parallel c$ axis and $H_{ab}^s \approx 27$ kOe for $H \parallel ab$ plane which suggests that the easy magnetization direction is along the c axis. Moreover, the saturation magnetic moments at 2 K is $M_c^s = 4.01\mu_B$ /formula for $H \parallel c$ axis, and $M_{ab}^s = 3.38\mu_B$ /formula for $H \parallel ab$ plane. These results are in good agreement with the previous report [8, 55]. The saturation magnetization for in-plane direction is lower than the out of plane direction which suggests the existence of a substantial amount of the AFM phase coexisting along with the dominant FM phase in the F3GT-1 sample [56].

Figure 3(c and d) shows the $M(H)$ curves of F3GT-2 in both directions at a few selected temperatures. The saturation applied field at $T = 2$ K, $H_c^s \approx 4$ kOe for $H \parallel c$ is much smaller than $H_{ab}^s \approx 40$ kOe for $H \parallel ab$, confirming the easy axis is the c axis. The saturation moment at $T = 2$ K is $M_c^s = 0.41\mu_B$ /f.u. for $H \parallel c$ and $M_{ab}^s = 0.38\mu_B$ /f.u. for $H \parallel ab$, respectively. Notably, F3GT-2 sample shows a significantly large coercive field of $H_c^c \approx 950$ Oe for $H \parallel c$ and $H_{ab}^c \approx 1550$ Oe for $H \parallel ab$ at 2 K, which are higher than the F3GT-1 [55]. The sudden slope change after reaching a certain critical field (15 kOe) a step-like feature appears that relates to the meta-magnetic transition [57, 58]. The obtained H_c for F3GT-2 is significantly larger than F3GT-1 at $T = 2$ K (almost 12 times). Whereas the saturation magnetization M_c^s is $0.41\mu_B$ /f.u. for $H \parallel c$, which is about ~ 10 order of magnitude lower than the F3GT-1. The value of M_s and H_c in both the directions for F3GT-1 and F3GT-2 are presented in tabular form in Table II.

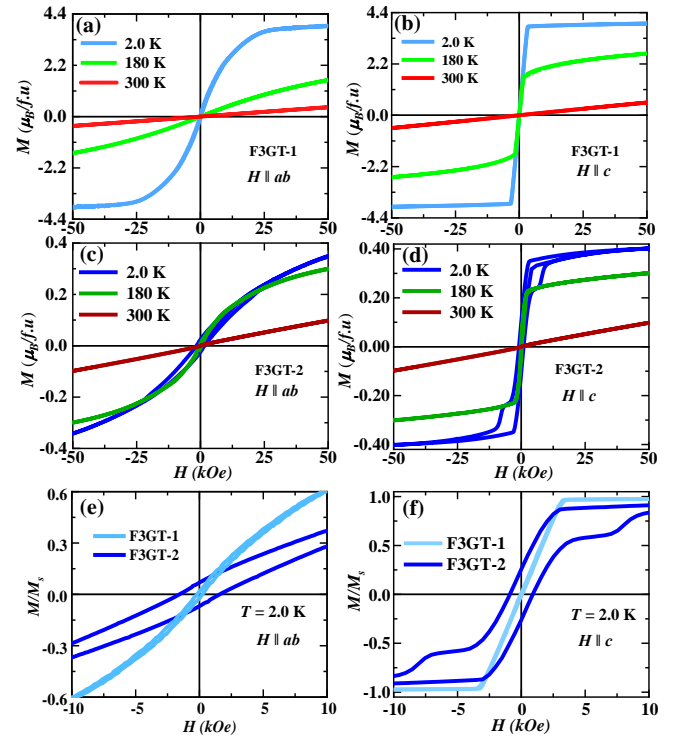


FIG. 3 Isothermal magnetization measurements. Isothermal magnetization at few selected temperatures measured in the ab plane and along the c axis for (a-b) F3GT-1 and (c-d) F3GT-2. (e-f) Normalized M/M_s at 2K for both samples shows significant enhancement of H_C and the emergence of metamagnetic feature in F3GT-2 with reference to F3GT-1.

The Rhodes-Wohlfarth ratio (RWR) is a very good criterion to ascribe whether the magnetic material belongs to the itinerant or a localized spin system. In the Stoner model, RWR is defined as μ_c/μ_s , where μ_c (μ_s)

TABLE II Saturation magnetization (M_s) and coercivity (H_c) of F3GT at $T \sim 2$ K. Shows significant enhancement of coercivity in F3GT-2.

Sample	Direction	M_s ($\mu_B/f.u$)	H_c (Oe)
F3GT-1	H c	4.01	45
	H ab	3.38	230
F3GT-2	H c	0.41	950
	H ab	0.38	1550

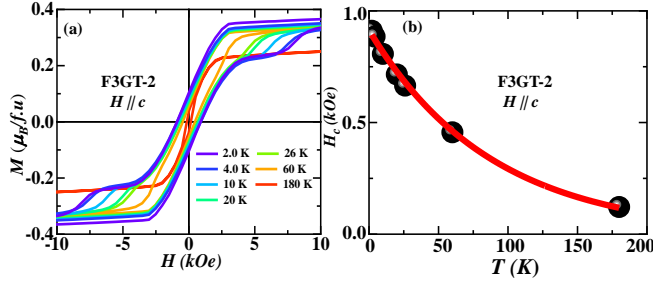


FIG. 4 Determination of coercive field, H_c of F3GT-2 from isothermal magnetization. (a)

Isothermal magnetization measured at various temperatures ($T=2, 4, 10, 20, 26, 60$ and 180 K) between ± 50 kOe for F3GT-2 ($H \parallel c$). (b) Coercive field (H_c) vs. temperature (T) plot and fits using equation 2 (red solid line) expected for spin glass/cluster spin glass systems.

+ 2) = μ_{eff}^2 and μ_s is the spontaneous magnetization in the ground state. RWR is 1 for a localized system and greater than 1 for an itinerant system. The RWR of F3GT-1 is found to be 3.25, while RWR of F3GT-2 is 5.52, suggesting itinerant character and/or strong spin fluctuations in the ground state[53].

Narrow $M(H)$ hysteresis loop with non-zero remanence and coercivity without saturation below T_C has been reported in spin-glasses/cluster spin glasses as well in superparamagnetic (SPM) systems [59–61]. A distinction between the $M(H)$ loops of spin-glasses/cluster spin-glass and SPM systems can be made through the study of the temperature variation of coercivity. Therefore, $M(H)$ hysteresis loops are recorded at various temperatures and presented in Figure 4(a). It is seen that temperature dependence of coercive field (H_c) determined from $M(H)$ loops is shown in Figure 4(b). The coercivity exponentially decreases with increasing temperature and follows the empirical relationship expected for spin glasses/cluster spin glasses below the transition temperature $T_C \sim 210$ K[61, 62]

$$H_c(T) = H_c(0) e^{-\alpha T} \quad (2)$$

where $H_c(0)$ is the coercive field at 0 K, while α is a fitting parameter. The solid line in Figure 4(b) is the

least squares fit using equation 2 with fitting parameters $H_c(0) = (911 \pm 14)$ Oe, $\alpha = (0.0112 \pm 0.0006)$ K^{-1} . The exponential dependence of H_c is regarded as the signature of spin glasses/cluster spin glasses[61].

3. Magnetic relaxation & ac susceptibility:

The above $M(T)$ and $M(H)$ results directly point towards the presence of disorder and/or frustrations in F3GT-2. To probe the stability of the zero-field magnetic state, magnetic relaxation at a few selected temperatures ($T = 25, 50, 100,$ and 150 K) are measured in the FCC condition and presented in Figure 5(a) [63]. The sample is first cooled from 300 K to the desired temperature in the presence of $H = 100$ Oe ($H \parallel c$) and M is measured as a function of time(t) immediately after removing the field. The magnitude of relaxation is found to increase with increasing T . After $t = 2$ h, the sample shows about 10% change in M at 150 K, which is enormous as far as the relaxation in other glassy and disordered systems are concerned [64]. This relaxation behavior can be fitted with a logarithmic relaxation function given by,

$$M(t) = M_0 + \alpha \log(t) \quad (3)$$

here M_0 is the initial magnetization and α is the relaxation rate in dynamic equilibrium[63, 65].

Although the logarithmic time dependence of isothermal remanent magnetization is normally associated with glassy magnetic system, it has also been observed in materials with complex interactions without spin-glass freezing. Therefore, to further check whether the relaxation is related to the formation of a glassy state, the temperature dependent AC susceptibility ($\chi_{ac}(T)$) measurement was performed in temperature regime from 240K to 75K at various frequencies (11 Hz, 111Hz, 587 Hz and 987 Hz) under an AC drive field of 4 Oe [63]. The real part of susceptibility, $\chi'_{ac}(T)$ exhibits anomaly. The amplitude and peak position depend on the frequency of the applied ac magnetic field. The maxima in $\chi'_{ac}(T)$ observes around 208.9 K at 11 Hz, shown in Figure 5(b), support the T_C peak in the dc magnetization curves. The position of maxima shifts towards the higher temperature as the frequency is increased, which further confirms the existence of a glassy magnetic phase. It is also observed that the amplitude of maxima in $\chi'_{ac}(T)$ decreases with increasing frequency. The Mydosh parameter is used as the criterion to categorize the glassy magnetic systems according to the response of magnetic spins compare the relative shift in freezing temperature per decade of frequency[66]. To understand the spin freezing dynamics, the Mydosh parameter is calculated followed by Vogel-Fulcher (VF) and critical slowing dynamics models [67]. The Mydosh parameter (K) is defined as

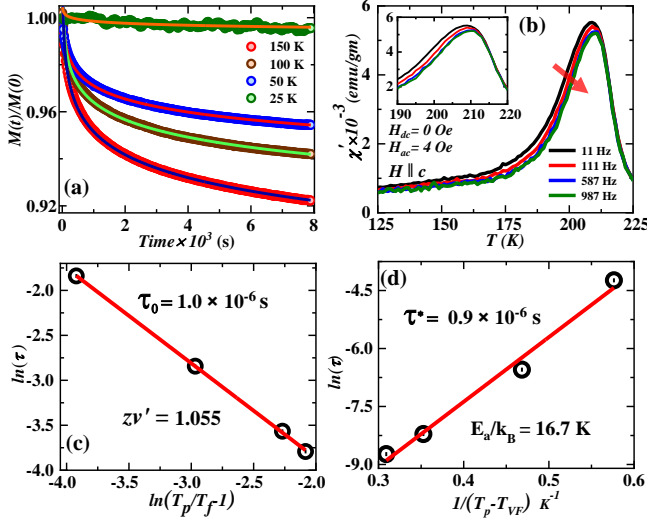


FIG. 5 Magnetic relaxation and the ac susceptibility ($\chi'_{ac}(T)$) (a) Relaxation of M at different temperatures after the field is withdrawn. The solid lines are fits with a logarithmic relaxation function (see equation 3). (b) The real parts of the ac magnetic susceptibility ($\chi'_{ac}(T)$) of F3GT-2 measured at a few selected frequencies from 11 Hz to 987 Hz in an applied ac magnetic field of 4 Oe along c -axis. (c) The relaxation time (τ) dependence of freezing temperature plotted as $\ln(\tau)$ vs $\ln(t)$. Here $t = (T_p - T_f)/T_f$ is reduced temperature. The solid line represents the fit to the power-law divergence. (d) Relaxation time (τ) vs freezing temperature plotted in log scale ($\ln(\tau)$ vs $1/(T_p - T_{VF})$) together with the fit using Vogel-Fulcher equation.

$$K = \frac{\Delta T_{pf}}{T_p \Delta(\log(f))} \quad (4)$$

where T_p represents the temperature where the AC susceptibility is maximum and f is the measured frequency. Here, $\Delta T_{pf} = T_{pf1} - T_{pf2}$ and $\Delta \log(f) = \log(f1) - \log(f2)$. The value of K is 0.004 which is comparable to the reported values for other Cluster Glass (CG) systems ($K \leq 0.08$) [68, 69].

The frequency dependence of T_p follows the conventional power-law divergence of critical slowing down,

$$\tau = \tau_0 \left(\frac{T_p - T_f}{T_f} \right)^{-z\nu'} \quad (5)$$

where τ is the relaxation time corresponding to the measured frequency ($\tau = 1/\nu$), τ_0 is the characteristic relaxation time of the individual spin cluster, T_f is the

freezing temperature for $\nu \rightarrow 0$ Hz, and $z\nu'$ is the dynamic critical exponent [ν' is the critical exponent of correlation length, $\xi = (T_p/T_f - 1)^{-\nu'}$ and the dynamical scaling relates τ to ξ as $\tau \sim \xi^z$] [70–72].

It is useful to rewrite equation 5 as

$$\ln(\tau) = \ln(\tau_0) - z\nu' \ln(t) \quad (6)$$

where $t = \frac{T_p - T_f}{T_f}$. The plot of $\ln(\tau)$ versus $\ln(t)$ is shown in the Figure 5(c), from the slope and intercept we can estimate the value of $z\nu'$ and τ_0 respectively. Obtained values of the characteristic relaxation τ_0 , $z\nu'$ and T_f are 1.0×10^{-6} s, 1.05 ± 0.05 and 208.88 K for this system [69]. However, the value of τ_0 is larger compared to the typical canonical spin glass systems ($\sim 10^{-12}$ s for). This suggests the possibility of strongly interacting clusters rather than individual spins [71] in F3GT-2, which gives a slow spin relaxation.

Further, the Vogel-Fulcher (VF) relaxation model has been used to analyze the behavior of interaction among the frozen spin clusters [71]. The interacting particles (or spin clusters) in a magnetic system undergoes a relaxation process in which the relaxation time follows the VF law given by,

$$\tau = \tau^* \exp\left(\frac{-E_a}{k_B(T_p - T_{VF})}\right) \quad (7)$$

where τ is the relaxation time, E_a is the activation energy, τ^* is the characteristic time between the relaxation attempts of spin clusters, and T_{VF} is the VF temperature, which provides inter-clusters interaction strength. We calculate the value of Vogel-Fulcher temperature T_{VF} by Souletie and Tholence method and obtain $T_{VF} = 207.16$ K, which we use to find τ^* and E_a . The linear fitted $\ln(\tau)$ versus $1/(T_p - T_{VF})$ curve is shown in the Figure 5(d). From the linear fitting parameter, we get $E_a/k_B = 16.7$ K and $\tau^* = 0.9 \times 10^{-6}$, which falls within the range of characteristic relaxation times for the cluster glass system. Thus, critical slowing down of dynamics and VF models along with the Mydosh parameter strongly support spin cluster glass behavior in F3GT-2.

IV. DISCUSSIONS

The structural analysis confirms the single-phase crystalline nature of F3GT-1, whereas it reveals the presence of a minor FT phase ($\lesssim 1.2\%$) in the F3GT-2 crystal. Presence of minor FT phase is further confirmed by the resistivity measurements, where a hump in resistivity at around 68 K (close to the reported $T_{C1} \sim 70$ K, see appendix C) is observed. The appearance of MI transition is direct evidence, as FT shows a similar nature at \sim

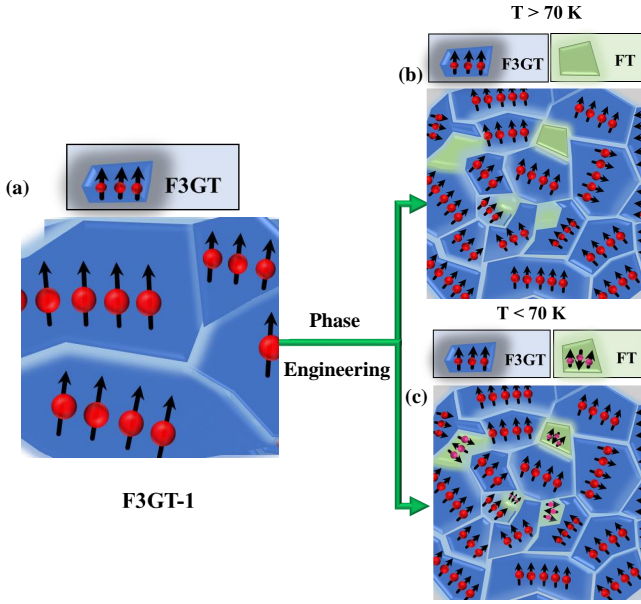


FIG. 6 Illustration of conventional cluster spin-glass in F3GT-2. The schematic diagram of (a) the pure F3GT-1 phase with a relatively smaller amount of multi-domain boundary and (b-c) F3GT-2 sample with a much higher amount of multi-domain boundary disorder above and below 70 K.

70 K [73, 74] and ordered antiferromagnetically at around 70 K [75].

Now based on all the above observations, a schematic micro-structure diagram describing the comparative scenarios of the two samples F3GT-1 and F3GT-2 has been proposed in Figure 6, where the FM and AFM phase domains are presented by light blue and green color respectively and arrow denotes the spin directions. The figure 6 (a) describes the pure F3GT-1 phase with a relatively smaller amount of multi-domain boundary disorder (small number of magnetic domains with different spin orientations), giving rise to relatively lower spin glass temperature (manifested by the onset of bifurcation in magnetic susceptibility at 182 K in figure 2 (a) and figure A3 (a-c) in appendix C).

The figure 6(b-c) describes the F3GT-2 sample with a much higher amount of multi-domain boundary disorder (larger number of magnetic domains in the figure), giving rise to much higher spin glass temperature (manifested by the onset of bifurcation in magnetic susceptibility at 215 K, figure 2 (c) of C). This explains the fundamental change induced by phase engineering, i.e., the increase in disorder and multi-domain formation due to the randomly embedded clusters of the co-planar FeTe (FT) phase, which serve as mosaic pinning centers between grains of F3GT. The presence of FT in F3GT acts as phase separation disorder that separates the FM domains of F3GT. The presence of disorder in the form of mosaic FT phase regions reduces the interdomain magnetic coupling and enhances the spin cluster glass behav-

ior in F3GT-2 [76–78]. This picture is also consistent with the SEM data, which shows relatively smooth terrain in F3GT-1 but enhanced granularity and the presence of FT phase hexagonal flakes in F3GT-2 as seen in figure A1.

The other comparative picture (figure 6(b-c) of F3GT-2) relates to the spin scenario of the same sample above and below T_{C1} (~ 70 K). Above T_{C1} the contribution of the FT phase domains is purely structural and non-magnetic disorder related. But below T_{C1} , the AFM spin texture also starts to contribute to the scenario, giving rise to the metamagnetic features observed in Fig 3 and figure 4. The strong anisotropic pinning forces across the anti-phase boundaries (APBs) of the anti-parallel domains offer a significant hindrance to the applied magnetic field (H) to orient them along the field direction [76–78]. On reaching a critical value of applied H, the magnetization suddenly increases in the form of steps and gives rise to a meta-magnetic transition.

V. CONCLUSION

We have demonstrated an effective way to enhance the coercivity in 2D vdW magnetic material, F3GT through phase engineering, in which the F3GT crystal has been infused with a very small amount of FeTe phase ($\lesssim 1.2\%$). This FT phase acts as both mosaic pinning centers between grains of F3GT above its antiferromagnetic transition temperature ($T_c1 \sim 70$ K) and also as anti-phase domains below T_{C1} . This results in increased grain boundary disorder and metastable nature, which leads to highly enhanced coercivity (≈ 1 kOe), cluster spin glass, and metamagnetic behavior. The enhanced coercivity makes F3GT-2 much more useful for memory storage applications and is likely to open a new direction toward the development of magnetic materials with higher coercivity and novel magnetic states for potential applications.

VI. ACKNOWLEDGEMENT

This work was supported by the (i) 'Department of Science and Technology', Government of India (Grant No. SRG/2019/000674 and EMR/2016/005437), and (ii) Collaborative Research Scheme (CRS) project proposal(2021/CRS/59/58/760). S.Bera & A.Bera thanks CSIR Govt. of India for Research Fellowship with Grant No. 09/080(1110)/2019-EMR-I & 09/080(1109)/2019-EMR-I, respectively. S.B. acknowledges the experimental facilities for sample growth, procured using financial support from DST-SERB grant nos. ECR/2017/002 037. The authors also would like to acknowledge Mr. Md Yousuf Sk, Prof. Subham Majumdar, and Dr. Subhadeep Datta for technical help and fruitful discussions.

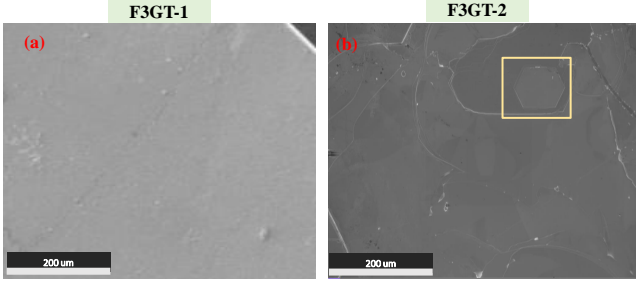


FIG. A1 Microstructural characterization. High-resolution SEM image of (a) F3GT-1 shows a relatively smaller amount of multi-domain boundary disorder, whereas the second image (b) of F3GT-2 shows a much higher amount of multi-domain boundary disorder.

Appendix A: Elemental composition analysis:SEM-EDX

Figure A1(a) describes the pure F3GT-1 phase with a relatively smaller amount of multi-domain boundary disorder, and the large area EDX (whose stoichiometry is mentioned in Section III A), was performed over the entire region enclosed by the figure whereas second figure A1(b) describes the F3GT-2 sample with a much higher amount of multi-domain boundary disorder. Here also, the large area EDX (whose stoichiometry is also mentioned in Section III A), was performed over the entire region enclosed by the figure, whereas a separate point EDX was performed on the hexagonal-shaped flake enclosed in the yellow-colored box. It revealed a clear Ge deficiency (Ge was found to be only 2%, which may have originated from the background as background has clear F3GT phase stoichiometry, i.e., molar ratio of Ge is close to 1.0). This is an indicator of FeTe phase with no Ge. Also, the flake area is very small compared to the background (which is consistent with the phase fraction $\sim 1.2\%$ obtained from XRD analysis in section III)

Appendix B: Resistivity

Temperature-dependent out-of-plane electrical resistivity [$\rho(T)$] of both F3GT-1 and F3GT-2 in the temperature (T) range from 5 K-300 K are depicted in Figure A2(a) and (b) respectively. Here the observations are as follows : (i) Continuous decrease of $\rho(T)$ with decreasing T suggests the typical metallic behavior ($d\rho/dT > 0$) in F3GT-1 sample[8, 55]. A clear anomaly; a change in slope has seen observed at $T \sim 183$ K, (coincide with the magnetic phase transition, described in the earlier section) due to spin disorders in the itinerant electrons[13, 52]. (ii) On the other side F3GT-2 shows similar metallic behavior. However, F3GT-2 shows two anomalies at around 68 K and 210 K (see

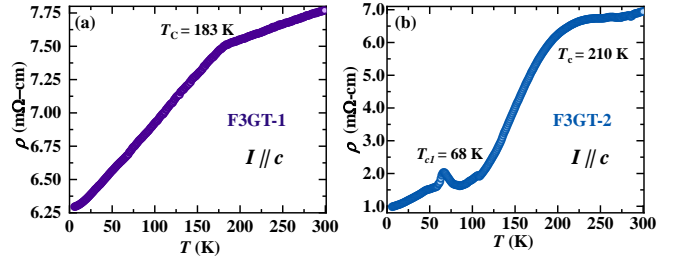


FIG. A2 Temperature-dependent electric transport measurement. The resistivity data of both samples are parented in (a) F3GT-1 and (b) F3GT-2. The transport study shows the FM transitions of both samples at around $200(\pm 10)$ K consistent with earlier reports. Whereas in addition to FM transition, F3GT-2 shows the signature of AFM transition of $FeTe$ at around 68 K.

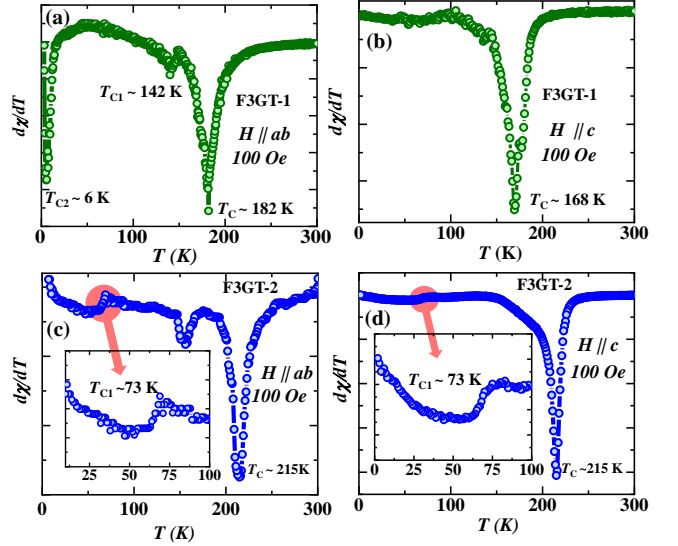


FIG. A3 The 1st derivative of $\chi_{dc}(T)$. The 1st derivative of $\chi_{dc}(T)$ in both direction of F3GT-1 and F3GT-2 are represent in (a-b) & (c-d) respectively.

Figure A2(b)). The anomaly around 210 K is consistent with the magnetic data ($M-T$) presented earlier. While the first anomaly (a sharp peak) at around 68 K signifies a metal-to-insulator type transition, that matches well with the previous report [52, 54].

Appendix C: Magnetization of F3GT sample

The 1st derivative of $\chi_{dc}(M/H)$ with respect to temperature of both sample along the ab plan and c -axis are presented in Figure A3. Two prominent deep ($T_C \sim 182$ K and $T_{C2} \sim 6$ K) and one small kink ($T_{C1} \sim 142$ K) just below the Ferromagnetic transition are observed along ab plan for F3GT-sample(see Figure A3(a)). Only ferromagnetic transition at 168 K is observed along the c -

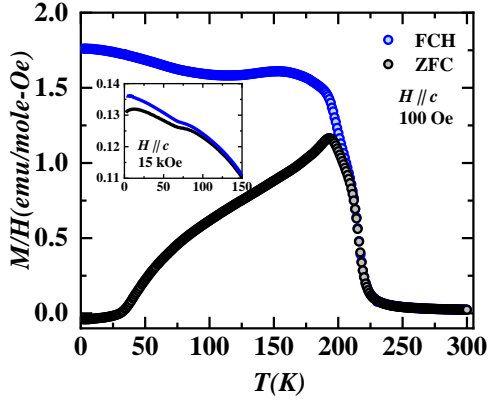


FIG. A4 Magnetization measurements. Temperature dependence of magnetization measures with the external magnetic field $H = 0.1$ kOe and 15 kOe applied along the c axis under zero-field-cooling (ZFC) and field-cool-heating (FCH) protocols for F3GT-2 single crystal.

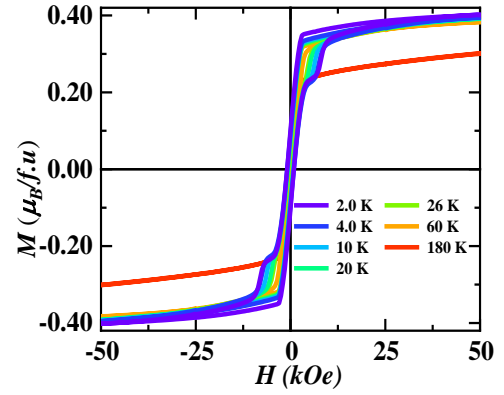


FIG. A5 Isothermal magnetization. Isothermal magnetization measured at different temperatures ($T=2, 4, 10, 20, 26, 60$ and 180 K) between ± 50 kOe for F3GT-2 at various temperatures ($H \parallel c$).

axis of F3GT-1 sample (see Figure A3(b)). On the other hand, similar kinds of features are noticed in the F3GT-2 sample (see Figure A3(c-d)). At around 73 K, a small kink is observed for F3GT-2 sample, which is probably due to induces FeTe phase in this system. Temperature dependence of magnetization measures with the external magnetic field $H = 0.1$ kOe and 15 kOe applied along the c axis under zero-field-cooling (ZFC) and field-cool-heating (FCH) protocols for F3GT-2 single crystal (see Figure A4). The bifurcation between FCH and ZFC data increases with decreasing values of applied external magnetic field [64].

Figure A5 shows isotherm magnetization at selected temperatures ($T=2, 4, 10, 20, 26, 60$ and 180 K) between ± 50 kOe for F3GT-2 at various temperatures ($H \parallel c$). The coercive field (H_C) and magnetic retentivity (M_C) decreases with increasing temperature.

-
- [1] S. Hirosawa, M. Nishino, and S. Miyashita, Perspectives for high-performance permanent magnets: applications, coercivity, and new materials, *Advances in Natural Sciences: Nanoscience and Nanotechnology* **8**, 013002 (2017).
- [2] Ferromagnetism, in *Introduction to Magnetic Materials* (John Wiley & Sons, Ltd, 2008) Chap. 4, pp. 115–149, <https://onlinelibrary.wiley.com/doi/pdf/10.1002/9780470386323.ch4>.
- [3] Z. Ding, L. Seyler Kyle, L. Xiayu, C. Ran, S. Nikhil, H. Bevin, S. Emma, T. Takashi, W. Kenji, A. McGuire Michael, Y. Wang, X. Di, C. Fu Kai-Mei, and X. Xiaodong, Van der waals engineering of ferromagnetic semiconductor heterostructures for spin and valleytronics, *Science Advances* **3**, e1603113 (2017).
- [4] B. Huang, G. Clark, E. Navarro-Moratalla, D. R. Klein, R. Cheng, K. L. Seyler, D. Zhong, E. Schmidgall, M. A. McGuire, D. H. Cobden, W. Yao, D. Xiao, P. Jarillo-Herrero, and X. Xu, Layer-dependent ferromagnetism in a van der waals crystal down to the monolayer limit, *Nature* **546**, 270 (2017).
- [5] C. Gong, L. Li, Z. Li, H. Ji, A. Stern, Y. Xia, T. Cao, W. Bao, C. Wang, Y. Wang, Z. Q. Qiu, R. J. Cava, S. G. Louie, J. Xia, and X. Zhang, Discovery of intrinsic ferromagnetism in two-dimensional van der waals crystals, *Nature* **546**, 265 (2017).
- [6] K. S. Burch, D. Mandrus, and J.-G. Park, Magnetism in two-dimensional van der waals materials, *Nature* **563**, 47 (2018).
- [7] A. Kabiraj, M. Kumar, and S. Mahapatra, High-throughput discovery of high curie point two-dimensional ferromagnetic materials, *npj Computational Materials* **6**, 35 (2020).
- [8] Y. Wang, C. Xian, J. Wang, B. Liu, L. Ling, L. Zhang, L. Cao, Z. Qu, and Y. Xiong, Anisotropic anomalous hall effect in triangular itinerant ferromagnet fe_3gete_2 , *Phys. Rev. B* **96**, 134428 (2017).
- [9] S. Mondal, N. Khan, S. M. Mishra, B. Satpati, and P. Mandal, Critical behavior in the van der waals itin-

- erant ferromagnet Fe_4GeTe_2 , *Phys. Rev. B* **104**, 094405 (2021).
- [10] S. Bera, S. K. Pradhan, M. S. Khan, R. Pal, B. Pal, S. Kalimuddin, A. Bera, B. Das, A. N. Pal, and M. Mondal, Unravelling the nature of spin reorientation transition in quasi-2d vdW magnetic material, Fe_4GeTe_2 , *Journal of Magnetism and Magnetic Materials* **565**, 170257 (2023).
- [11] A. F. May, M.-H. Du, V. R. Cooper, and M. A. McGuire, Tuning magnetic order in the van der Waals metal Fe_5GeTe_2 by cobalt substitution, *Phys. Rev. Materials* **4**, 074008 (2020).
- [12] J. Yi, H. Zhuang, Q. Zou, Z. Wu, G. Cao, S. Tang, S. A. Calder, P. R. C. Kent, D. Mandrus, and Z. Gai, Competing antiferromagnetism in a quasi-2d itinerant ferromagnet: Fe_3GeTe_2 , *2D Materials* **4**, 011005 (2016).
- [13] B. Chen, J. Yang, H. Wang, M. Imai, H. Ohta, C. Michioka, K. Yoshimura, and M. Fang, Magnetic properties of layered itinerant electron ferromagnet Fe_3GeTe_2 , *Journal of the Physical Society of Japan* **82**, 124711 (2013), <https://doi.org/10.7566/JPSJ.82.124711>.
- [14] Y. Liu and C. Petrovic, Three-dimensional magnetic critical behavior in CrI_3 , *Phys. Rev. B* **97**, 014420 (2018).
- [15] S. Son, M. J. Coak, N. Lee, J. Kim, T. Y. Kim, H. Hamidov, H. Cho, C. Liu, D. M. Jarvis, P. A. C. Brown, J. H. Kim, C.-H. Park, D. I. Khomskii, S. S. Saxena, and J.-G. Park, Bulk properties of the van der Waals hard ferromagnet V_3S_5 , *Phys. Rev. B* **99**, 041402 (2019).
- [16] M. A. McGuire, G. Clark, S. KC, W. M. Chance, G. E. Jellison, V. R. Cooper, X. Xu, and B. C. Sales, Magnetic behavior and spin-lattice coupling in cleavable van der Waals layered CrCl_3 crystals, *Phys. Rev. Materials* **1**, 014001 (2017).
- [17] A. K. Geim and I. V. Grigorieva, Van der Waals heterostructures, *Nature* **499**, 419 (2013).
- [18] A. K. Geim and K. S. Novoselov, The rise of graphene, *Nature Materials* **6**, 183 (2007).
- [19] K. S. Novoselov, D. Jiang, F. Schedin, T. J. Booth, V. V. Khotkevich, S. V. Morozov, and A. K. Geim, Two-dimensional atomic crystals, *Proceedings of the National Academy of Sciences* **102**, 10451 (2005), <https://www.pnas.org/doi/pdf/10.1073/pnas.0502848102>.
- [20] J.-X. Zhu, M. Janoschek, D. S. Chaves, J. C. Cezar, T. Durakiewicz, F. Ronning, Y. Sassa, M. Mansson, B. L. Scott, N. Wakeham, E. D. Bauer, and J. D. Thompson, Electronic correlation and magnetism in the ferromagnetic metal Fe_3GeTe_2 , *Phys. Rev. B* **93**, 144404 (2016).
- [21] Z. Yun, L. Haiyan, Z. Xiegang, T. Shiyong, F. Wei, L. Qin, Z. Wen, C. Qiuyun, L. Yi, L. Xuebing, X. Donghua, L. Lizhu, Z. Zhengjun, and L. Xinchun, Emergence of kondo lattice behavior in a van der Waals itinerant ferromagnet, Fe_3GeTe_2 , *Science Advances* **4**, eaao6791 (2021).
- [22] G. D. Nguyen, J. Lee, T. Berlijn, Q. Zou, S. M. Hus, J. Park, Z. Gai, C. Lee, and A.-P. Li, Visualization and manipulation of magnetic domains in the quasi-two-dimensional material Fe_3GeTe_2 , *Phys. Rev. B* **97**, 014425 (2018).
- [23] D. Weber, A. H. Trout, D. W. McComb, and J. E. Goldberger, Decomposition-induced room-temperature magnetism of the Na-intercalated layered ferromagnet Fe_3GeTe_2 , *Nano Lett.* **19**, 5031 (2019).
- [24] H. Iturriaga, L. M. Martinez, T. T. Mai, M. Augustin, A. R. H. Walker, M. F. Sanad, S. T. Sreenivasan, Y. Liu, E. J. G. Santos, C. Petrovic, and S. R. Singamaneni, Room temperature ferromagnetism in intercalated Fe_3GeTe_2 van der Waals magnet (2022).
- [25] L. Zhang, X. Huang, H. Dai, M. Wang, H. Cheng, L. Tong, Z. Li, X. Han, X. Wang, L. Ye, and J. Han, Proximity-coupling-induced significant enhancement of coercive field and Curie temperature in 2d van der Waals heterostructures, *Advanced Materials* **32**, 2002032 (2020), <https://onlinelibrary.wiley.com/doi/pdf/10.1002/adma.202002032>.
- [26] N. León-Brito, E. D. Bauer, F. Ronning, J. D. Thompson, and R. Movshovich, Magnetic microstructure and magnetic properties of uniaxial itinerant ferromagnet Fe_3GeTe_2 , *Journal of Applied Physics* **120**, 083903 (2016), <https://doi.org/10.1063/1.4961592>.
- [27] L. Fallarino, M. Quintana, E. López Rojo, and A. Berger, Suppression of coercivity in nanoscale graded magnetic materials, *Phys. Rev. Applied* **16**, 034038 (2021).
- [28] G. Fang Liu, Z. Dong Zhang, F. Dang, C. Bing Cheng, C. Xin Hou, and S. Da Liu, Formation and characterization of magnetic barium ferrite hollow fibers with low coercivity via co-electrospun, *Journal of Magnetism and Magnetic Materials* **412**, 55 (2016).
- [29] L. Zhu, S. Nie, K. Meng, D. Pan, J. Zhao, and H. Zheng, Multifunctional 110-mn1.5ga films with ultrahigh coercivity, giant perpendicular magnetocrystalline anisotropy and large magnetic energy product, *Advanced Materials* **24**, 4547 (2012), <https://onlinelibrary.wiley.com/doi/pdf/10.1002/adma.201200805>.
- [30] Z. Zhao, W. Li, Y. Zeng, X. Huang, C. Yun, B. Zhang, and Y. Hou, Structure engineering of 2d materials toward magnetism modulation, *Small Structures* **2**, 2100077 (2021), <https://onlinelibrary.wiley.com/doi/pdf/10.1002/ssstr.202100077>.
- [31] P. Wang, J. Ge, J. Li, Y. Liu, Y. Xu, and J. Wang, Intrinsic magnetic topological insulators, *The Innovation* **2**, 100098 (2021).
- [32] Y. Niu, J. Villalva, R. Frisenda, G. Sanchez-Santolino, L. Ruiz-González, E. M. Pérez, M. García-Hernández, E. Burzuri, and A. Castellanos-Gomez, Mechanical and liquid phase exfoliation of cylindrite: a natural van der Waals superlattice with intrinsic magnetic interactions, *2D Materials* **6**, 035023 (2019).
- [33] H. L. Feng, Z. Deng, M. Wu, M. Croft, S. H. Lapidus, S. Liu, T. A. Tyson, B. D. Ravel, N. F. Quackenbush, C. E. Frank, C. Jin, M.-R. Li, D. Walker, and M. Greenblatt, High-pressure synthesis of $\text{Lu}_2\text{Ni}_2\text{O}_6$ with ferrimagnetism and large coercivity, *Inorg. Chem.* **58**, 397 (2019).
- [34] S. Ahmed, X. Ding, P. P. Murmu, N. Bao, R. Liu, J. Kennedy, L. Wang, J. Ding, T. Wu, A. Vinu, and J. Yi, High coercivity and magnetization in WSe_2 by codoping Co and Nb, *Small* **16**, 1903173 (2020), <https://onlinelibrary.wiley.com/doi/pdf/10.1002/smll.201903173>.
- [35] S. Ahmed, X. Ding, N. Bao, P. Bian, R. Zheng, Y. Wang, P. P. Murmu, J. V. Kennedy, R. Liu, H. Fan, K. Suzuki, J. Ding, and J. Yi, Inducing high coercivity in MoS_2 nanosheets by transition element doping, *Chem. Mater.* **29**, 9066 (2017).
- [36] H. Chang, Y. Lee, P. Liao, and W. Chang, Significant coercivity enhancement of hot deformed NdFeB magnets by doping Ce-containing (PrNdCe)70Cu30 alloys powders, *Scripta Materialia* **146**, 222 (2018).
- [37] S. Ahmed, X.-Y. Carl Cui, X. Ding, P. P. Murmu,

- N. Bao, X. Geng, S. Xi, R. Liu, J. Kennedy, T. Wu, L. Wang, K. Suzuki, J. Ding, X. Chu, S. R. Clastinrus-selraj Indirathankam, M. Peng, A. Vinu, S. P. Ringer, and J. Yi, Colossal magnetization and giant coercivity in ion-implanted (nb and co) mos2 crystals, *ACS Appl. Mater. Interfaces* **12**, 58140 (2020).
- [38] J. Dho, E. K. Lee, J. Y. Park, and N. H. Hur, Effects of the grain boundary on the coercivity of barium ferrite bafe12o19, *Journal of Magnetism and Magnetic Materials* **285**, 164 (2005).
- [39] B. H. Liu and J. Ding, Strain-induced high coercivity in cofe2o4 powders, *Applied Physics Letters* **88**, 042506 (2006), <https://doi.org/10.1063/1.2161808>.
- [40] X. H. Tan, S. F. Chan, K. Han, and H. Xu, Combined effects of magnetic interaction and domain wall pinning on the coercivity in a bulk nd60fe30al10 ferromagnet, *Scientific Reports* **4**, 6805 (2014).
- [41] C. Zhang, Y. Xie, Q. Zhan, and Y. Hu, Anisotropic coercivity and the effects of interlayer exchange coupling in cofeb/ferh bilayers, *Phys. Rev. B* **103**, 014445 (2021).
- [42] P. C. Rout and U. Schwingenschlöggl, Large magnetocrystalline anisotropy and giant coercivity in the ferrimagnetic double perovskite lu2niro6, *Nano Lett.* **21**, 6807 (2021).
- [43] S. Bhanuchandar, G. Vinothkumar, P. Arunkumar, M. Sribalaji, A. K. Keshri, and K. Suresh Babu, Controlled growth of ni/nio composite nanoparticles and its influence on exchange anisotropy and spin glass features, *Journal of Alloys and Compounds* **780**, 256 (2019).
- [44] C. Pereira, A. M. Pereira, C. Fernandes, M. Rocha, R. Mendes, M. P. Fernández-García, A. Guedes, P. B. Tavares, J.-M. Grenèche, J. P. Araújo, and C. Freire, Superparamagnetic mfe2o4 (m = fe, co, mn) nanoparticles: Tuning the particle size and magnetic properties through a novel one-step coprecipitation route, *Chem. Mater.* **24**, 1496 (2012).
- [45] D. J. Amit, H. Gutfreund, and H. Sompolinsky, Spin-glass models of neural networks, *Phys. Rev. A* **32**, 1007 (1985).
- [46] J. D. Bryngelson and P. G. Wolynes, Spin glasses and the statistical mechanics of protein folding., *Proceedings of the National Academy of Sciences* **84**, 7524 (1987), <https://www.pnas.org/doi/pdf/10.1073/pnas.84.21.7524>.
- [47] F. Pázmándi, G. Zaránd, and G. T. Zimányi, Self-organized criticality in the hysteresis of the sherrington-kirkpatrick model, *Phys. Rev. Lett.* **83**, 1034 (1999-08).
- [48] P. Guardia, A. Labarta, and X. Batlle, Tuning the size, the shape, and the magnetic properties of iron oxide nanoparticles, *J. Phys. Chem. C* **115**, 390 (2011).
- [49] A. G. Kolhatkar, A. C. Jamison, D. Litvinov, R. C. Willson, and T. R. Lee, Tuning the magnetic properties of nanoparticles, *International Journal of Molecular Sciences* **14**, 15977 (2013).
- [50] A. Sultan, T. Cheng, C. Zhong-Jia, G. Partridge James, Z. Guolin, F. Lawrence, H. Mayes Edwin L., R. Field Matthew, L. Changgu, W. Yihao, X. Yiming, T. Mingliang, X. Feixiang, R. Hamilton Alex, A. Tretiakov Oleg, C. Dimitrie, Z. Yu-Jun, and W. Lan, Antisymmetric magnetoresistance in van der waals fe3gete2/graphite/fe3gete2 trilayer heterostructures, *Science Advances* **5**, eaaw0409 (2021).
- [51] S. Junho, K. D. Young, A. E. Su, K. Kyoo, K. Gi-Yeop, H. Soo-Yoon, K. D. Wook, J. B. Gyu, K. Hee-jung, E. Gyeongsik, S. S. Young, S. Roland, M. Matthias, L. Jinwon, W. Kenji, T. Takashi, J. Y. Jung, L. Jieun, M. B. Il, J. M. Ho, Y. H. Woong, C. Si-Young, S. J. Hoon, and K. J. Sung, Nearly room temperature ferromagnetism in a magnetic metal-rich van der waals metal, *Science Advances* **6**, eaay8912 (2021).
- [52] Q. Mao, B. Chen, J. Yang, Y. Zhang, H. Wang, and M. Fang, Critical properties of the quasi-two-dimensional metallic ferromagnet fe2.85gete2, *Journal of Physics: Condensed Matter* **30**, 345802 (2018).
- [53] Y. Liu, V. N. Ivanovski, and C. Petrovic, Critical behavior of the van der waals bonded ferromagnet fe3-xgete2, *Phys. Rev. B* **96**, 144429 (2017).
- [54] J. Jiang, C. He, Y. Zhang, M. Xu, Q. Q. Ge, Z. R. Ye, F. Chen, B. P. Xie, and D. L. Feng, Distinct in-plane resistivity anisotropy in a detwinned fete single crystal: Evidence for a hund's metal, *Phys. Rev. B* **88**, 115130 (2013).
- [55] Y. Liu, E. Stavitski, K. Attenkofer, and C. Petrovic, Anomalous hall effect in the van der waals bonded ferromagnet fe3-xgete2, *Phys. Rev. B* **97**, 165415 (2018).
- [56] I. M. Fita, R. Szymczak, M. Baran, V. Markovich, R. Puzniak, A. Wisniewski, S. V. Shiryayev, V. N. Varyukhin, and H. Szymczak, Evolution of ferromagnetic order in lamno3.05 single crystals: Common origin of both pressure and self-doping effects, *Phys. Rev. B* **68**, 014436 (2003).
- [57] S. P. Bennett, A. T. Wong, A. Glavic, A. Herklotz, C. Urban, I. Valmianski, M. D. Biegalski, H. M. Christen, T. Z. Ward, and V. Lauter, Giant controllable magnetization changes induced by structural phase transitions in a metamagnetic artificial multiferroic, *Scientific Reports* **6**, 22708 (2016).
- [58] J. K. Murthy, K. D. Chandrasekhar, H. C. Wu, H. D. Yang, J. Y. Lin, and A. Venimadhav, Metamagnetic behaviour and effect of field cooling on sharp magnetization jumps in multiferroic y2comno6, *EPL (Europhysics Letters)* **108**, 27013 (2014-10).
- [59] Q. Dong, B. Shen, J. Chen, J. Shen, and J. Sun, Spin-glass behavior and magnetocaloric effect in melt-spun tbcual alloys, *Solid State Communications* **151**, 112 (2011).
- [60] M. Vafaei, S. Finizio, H. Deniz, D. Hesse, H. Zabel, G. Jakob, and M. Kläui, The effect of interface roughness on exchange bias in la0.7sr0.3mno3-bifeo3 heterostructures, *Applied Physics Letters* **108**, 072401 (2016), <https://doi.org/10.1063/1.4941795>.
- [61] M. K. Sharma and K. Mukherjee, Evidence of large magnetic cooling power and double glass transition in tb5pd2, *Journal of Magnetism and Magnetic Materials* **466**, 317 (2018).
- [62] A. Kumar and D. Pandey, Study of magnetic relaxation, memory and rejuvenation effects in the cluster spin-glass phase of b-site disordered ca(fe1/2nb1/2)o3 perovskite: Experimental evidence for hierarchical model, *Journal of Magnetism and Magnetic Materials* **511**, 166964 (2020).
- [63] N. K. Singh, D. Paudyal, Y. Mudryk, V. K. Pecharsky, and K. A. Gschneidner, Magnetostructural properties of ho5(Si0.8Ge0.2)4, *Phys. Rev. B* **81**, 184414 (2010).
- [64] S. Chatterjee, P. Dutta, S. Giri, S. Majumdar, S. Sadhukhan, S. Kanungo, S. Chatterjee, M. M. Patidar, G. S. Okram, and V. Ganesan, Glassy magnetic state and negative temperature coefficient of resistivity in mn3+δIn, *Phys. Rev. B* **102**, 214443 (2020).
- [65] V. K. Anand, D. T. Adroja, and A. D. Hillier, Ferro-

- magnetic cluster spin-glass behavior in prrhsn_3 , PRB **85**, 014418 (2012).
- [66] C. A. M. Mulder, A. J. van Duynveldt, and J. A. Mydosh, Susceptibility of the CuMn spin-glass: Frequency and field dependences, Phys. Rev. B **23**, 1384 (1981).
- [67] C. S. Yadav, S. K. Pandey, and P. L. Paulose, Evolution of magnetic ordering in $\text{fcr}_2\text{se}_{4-x}\text{te}_x$; $x = 0 - 4.0$ (2019).
- [68] R. R. Das, P. Parida, A. K. Bera, T. Chatterji, B. R. K. Nanda, and P. N. Santhosh, Giant exchange bias in the single-layered ruddlesden-popper perovskite $\text{SrLaCo}_{0.5}\text{Mn}_{0.5}\text{O}_4$, PRB **98**, 184417 (2018).
- [69] A. V. K., R. R. Das, P. Neenu Lekshmi, R. Dhal, C. V. Colin, and P. N. Santhosh, Giant exchange bias effect in ruddlesden-popper oxides $\text{srlafe}_{0.25+x}\text{mn}_{0.25}\text{co}_{0.5-x}\text{o}_4$ ($x = 0, 0.25$): Role of the cluster glass magnetic phase in a quasi-two-dimensional perovskite, Phys. Rev. B **102**, 134405 (2020).
- [70] M. D. Mukadam, S. M. Yusuf, P. Sharma, S. K. Kulshreshtha, and G. K. Dey, Dynamics of spin clusters in amorphous fe_2o_3 , PRB **72**, 174408 (2005).
- [71] V. K. Anand, D. T. Adroja, and A. D. Hillier, Ferromagnetic cluster spin-glass behavior in prrhsn_3 , Phys. Rev. B **85**, 014418 (2012).
- [72] J. A. Mydosh, Spin glasses: redux: an updated experimental/materials survey, Reports on Progress in Physics **78**, 052501 (2015).
- [73] L. Kang, C. Ye, X. Zhao, X. Zhou, J. Hu, Q. Li, D. Liu, C. M. Das, J. Yang, D. Hu, J. Chen, X. Cao, Y. Zhang, M. Xu, J. Di, D. Tian, P. Song, G. Kutty, Q. Zeng, Q. Fu, Y. Deng, J. Zhou, A. Ariando, F. Miao, G. Hong, Y. Huang, S. J. Pennycook, K.-T. Yong, W. Ji, X. Renshaw Wang, and Z. Liu, Phase-controllable growth of ultrathin 2d magnetic fete crystals, Nature Communications **11**, 3729 (2020).
- [74] P. K. Maheshwari, R. Jha, B. Gahtori, and V. P. S. Awana, Structural and magnetic properties of flux-free large fete single crystal, Journal of Superconductivity and Novel Magnetism **28**, 2893 (2015).
- [75] Y. Kim, S. Huh, J. Kim, Y. Choi, and C. Kim, Magnetic field detwinning in fete, Progress in Superconductivity and Cryogenics **21**, 6 (2019).
- [76] K. Anand, A. Pal, M. Alam, S. Dan, S. Kumar, S. Ghosh, S. Kumari, A. Das, M. Sawada, A. Mohan, V. G. Sathe, and S. Chatterjee, Emergence of metamagnetic transition, re-entrant cluster glass and spin phonon coupling in $\text{tb}_2\text{comno}_6$, Journal of Physics: Condensed Matter **33**, 275802 (2021).
- [77] J. Blasco, J. García, G. Subías, J. Stankiewicz, J. A. Rodríguez-Velamazán, C. Ritter, J. L. García-Muñoz, and F. Fauth, Magnetoelectric and structural properties of y_2CoMn_6 : The role of antisite defects, Phys. Rev. B **93**, 214401 (2016).
- [78] Y. Liu, R. J. Koch, Z. Hu, N. Aryal, E. Stavitski, X. Tong, K. Attenkofer, E. S. Bozin, W. Yin, and C. Petrovic, Three-dimensional ising ferrimagnetism of cr-fe-cr trimers in Fecr_2te_4 , Phys. Rev. B **102**, 085158 (2020).